

Spectroscopic Signatures of Conduction-Mediated Transition Layers Above an X-ray Illuminated Disk

Yuxing Li, Ming F. Gu^{1,2}, and Steven M. Kahn

Columbia Astrophysics Laboratory, Columbia University, New York, NY 10027

yxli@astro.columbia.edu, mfgu@space.mit.edu, skahn@astro.columbia.edu

Received _____; accepted _____

¹Chandra Fellow

²Now at: Center for Space Research, Massachusetts Institute of Technology, Cambridge, MA 02139

ABSTRACT

We derive a semi-analytic solution for the structure of conduction-mediated transition layers above an X-ray illuminated accretion disk, and calculate explicitly the X-ray line radiation resulting from both resonance line scattering and radiative recombination in these layers. The vertical thermal structure of the illuminated disk is found to depend on the illuminating continuum: for a hard power law continuum, there are two stable phases connected by a single transition layer; while for a softer continuum, there may exist three stable phases connected by two separate transition layers, with an intermediate stable layer in between. We show that the structure can be written as a function of the electron scattering optical depth through these layers, which leads to unique predictions of the equivalent width of the resulting line radiation from both recombination cascades and resonance line scattering. We find that resonance line scattering plays an important role, especially for the case where there is no intermediate stable layer.

Subject headings: accretion disks – galaxies:nuclei – radiative transfer – resonant scattering – X-rays:spectra

1. INTRODUCTION

X-ray reflection off the surface of cold disks in active galactic nuclei (AGN) and galactic black holes (GBHs) has been an active field of research since the work of Lightman & White (1988). In early studies, the illuminated material was assumed to be cold and non-ionized (Lightman & White 1988; George & Fabian 1991). It was soon realized, however, that photoionization of the disk can have a great impact on both the reflected continuum and the iron fluorescence lines. Detailed calculations were then carried out by Ross & Fabian (1993); Matt, Fabian & Ross (1993); Źycki et al. (1994); Ross, Fabian & Brandt (1996) and Ross, Fabian & Young (1999). However, in all of these papers, the density of the illuminated material was assumed to be constant along the vertical direction. This assumption applies only to the simplest version of radiation-dominated Shakura-Sunyaev disks (Shakura & Sunyaev 1973), and only for the portion where viscous dissipation is the dominating heating process. For the surface layers, however, photoionization and Compton scattering are the major heating sources. Therefore the approximation of constant density is not appropriate. Moreover, thermal instability allows the coexistence of gas at different phases. These different phases have very different temperatures, and hence different densities to keep the gas in pressure balance.

Recently Nayakshin, Kazanas & Kallman (2000) relaxed the simplifying assumption of constant gas density. They determined the gas density from hydrostatic balance solved simultaneously with ionization balance and radiative transfer. They made an important observation that the Thomson depth of the hot coronal layer can have great influence on the X-ray reprocessing produced by the deeper, and much cooler disk. In order to simplify the calculation of the vertical structure, though, they ignored thermal conduction and the effects of transition layers between the different stable phases. A discontinuous change in temperature was allowed whenever an unstable phase was encountered. They argued that

such transition layers are of little importance because their Thomson depths are negligibly small. However, without taking into account the role of thermal conduction, their method of connecting two different stable layers is rather *ad hoc*. Moreover, even though the Thomson depths of these transition layers are small, it does not guarantee that the X-ray emission and reflection from such layers are negligible. Because the temperature regime where the transition layers exist is not encountered in the stable phases, some of the most important lines can have appreciable emissivity only in these layers. Also, since resonance line scattering has much larger cross section than Thomson scattering, the optical depths in resonance lines can be significant.

Including thermal conduction in the self-consistent solution of the vertical structure presents a serious numerical challenge. The difficulties are due to the coupling between hydrostatic balance, radiative transfer and heat conduction. Zel'dovich & Pikel'ner (1969) first studied the phase equilibrium of a gas heated by cosmic rays and cooled by radiation. They found that taking into account heat conduction in the boundary layer allows one to obtain a unique solution of the stable equilibrium. Różańska (1999) calculated the full temperature profile for a Compton-heated corona, and Różańska & Czerny (2000a) calculated the static conditions of the plasma for different forms of heating and cooling. But they did not include much discussion of the spectroscopic signatures resulting from the derived vertical structure.

In this paper, we first calculate the temperature structure in the layers above the accretion disk, then calculate the emission lines via radiative recombination (RR) and reflection due to resonance line scattering from the derived layers. Certain illuminating continua spectra allow more than two stable phases to coexist, with two transition layers connected by an intermediate stable layer. For the transition layer, since the Thomson depth is small, the ionizing continuum can be treated as constant; and since its geometric

thickness is smaller than the pressure scale height, the pressure can be treated as constant as well. We can thus obtain semi-analytic solution of the temperature profile by taking into account thermal conduction. For the intermediate stable layer, its thickness is determined by the condition of hydrostatic equilibrium. In our model, the normally incident continuum has a power-law spectrum with an energy index of $\alpha = 1$. We also assume a plane-parallel geometry and that the resonance line scattering is isotropic.

The structure of this paper is as follows: In §2 we discuss the existence of the thermal instability and compute the thermal ionization structure of the transition layers; in §3 we calculate the recombination emission lines and the reflection due to resonance line scattering; in §4 we summarize the important points of the calculations, the validity of various approximations made in the calculations, and the detectability of the recombination emission and reflection lines.

2. THERMAL INSTABILITY AND TRANSITION LAYERS

2.1. The “S curves”

The vertical structure of an X-ray illuminated disk at rest is governed by the equations of hydrostatic equilibrium and of energy conservation

$$\frac{dP}{dx} = -n_H(x)F, \quad (1)$$

$$-\frac{d}{dx}(\kappa(T)\frac{dT}{dx}) = \Phi(T, P, F_x(E)). \quad (2)$$

In the first equation, F is the force density due to gravity and radiation pressure. The dependence of the force on the plasma density is included explicitly through the hydrogen density $n_H(x)$. In the second equation, a time independent state is assumed, $\kappa(T)$ is the thermal conductivity, and $\Phi(T, P, F_x(E))$ is the net heating rate depending on the gas state and the incident flux $F_x(E)$ (differential in energy). We neglect the effects of

magnetic field and adopt the Spitzer conductivity appropriate for a fully ionized plasma, $\kappa(T) = 5.6 \times 10^{-7} T^{5/2} \text{ erg cm}^2 \text{ s}^{-1} \text{ K}^{-1}$ (Spitzer 1962). We have used the classical heat flux, $q_{class} = -\kappa(T)\nabla T$, in Equation (2) because the electron mean free path is short compared to the temperature height scale.

Since the continuum flux may change along the vertical height, in principle, the above two equations must be supplemented by an equation for radiative transfer. A self-consistent solution of such equations is difficult to obtain. In the following, we invoke a few physically motivated approximations, which make the problem tractable.

First, in thermally stable regions, the gas temperature is slowly varying, the heat conduction term in the energy balance equation can be neglected. Therefore, the temperature can be determined locally with the condition $\Phi(T, P, F_x(E)) = 0$. It is well known (Krolik, McKee & Tarter 1981) that the dependence of Φ on the gas pressure P and the illuminating continuum $F_x(E)$ can be expressed in the form of $\Phi = -n_e^2 \Lambda_{net}(T, \Xi)$, where n_e is the electron density, $\Lambda_{net}(T, \Xi)$ is the net cooling rate per unit volume, and Ξ is an ionization parameter defined by

$$\Xi = \frac{F_x}{cP}, \quad (3)$$

where F_x is the total flux of the continuum, and c is the speed of light. In Figure 1, we show the local energy equilibrium curve T versus Ξ , at $\Lambda_{net}(T, \Xi) = 0$ calculated with the photoionization code XSTAR (Kallman & Krolik 1986). These curves are commonly referred to as “S curves” due to their appearance. The illuminating continuum is assumed to be a power law with energy index $\alpha = 1$. The solid line labeled with “S-curve 1” corresponds to a low energy cutoff at 1 eV and a high energy cutoff at 150 keV, while the dashed line “S-curve 2” corresponds to a high energy cutoff at 200 keV. The choice of such incident spectra is based on their common appearance in many AGNs and GBHCs. The region is thermally “unstable” where the “S-curve” has a negative slope, and “stable” where

the slope is positive, as indicated in Figure 1. In the thermally unstable regions, we have

$$\left(\frac{\partial \Xi}{\partial T} \right)_{\Lambda_{net}=0} < 0, \quad (4)$$

where the derivative is taken while the energy balance is satisfied, i.e., $\Lambda_{net} = 0$. This condition was shown (Krolik, McKee & Tarter 1981) to be equivalent to the instability condition discovered by Field (1965)

$$\left(\frac{\partial \Lambda_{net}}{\partial T} \right)_P < 0. \quad (5)$$

EDITOR: PLACE FIGURE 1 HERE.

2.2. The Temperature Profiles

2.2.1. The Transition layers

The thermal instability allows the gas to coexist at different phases. The gas temperature may change by orders of magnitude over a geometric thin region whenever an unstable phase separates two stable ones. This results in enormous temperature gradients and heat conduction. Therefore the heat conduction in the energy balance equation should be included in such transition layers between stable phases. On the other hand, the thicknesses of these transition layers are usually smaller than the pressure scale height, so one can safely treat the gas pressure as constant in these regions. Moreover, the continuum radiative transfer can be neglected because the Compton optical depth is found to be small. The vertical structure of the transition regions is then solely determined by the energy balance equation with heat conduction. The Thomson optical depth $d\tau_e = n_e \sigma_T dx$ of such regions is readily estimated by

$$\Delta\tau_e = \frac{\kappa(T)T\sigma_T}{\sqrt{\Lambda_{net}(T, \Xi)}}. \quad (6)$$

where σ_T is the Thomson scattering cross section.

The transition layer solution is not arbitrary under the steady-state conditions, i.e., where there is no mass exchange between the two stable phases which the transition layer connects. A similar problem in the context of interstellar gas heated by cosmic rays was well studied by Zel'dovich & Pikel'ner (1969). We follow their procedure here and define $y = \kappa(T)dT/d\tau_e$, in order to rewrite Equation (2) in the form:

$$\frac{dy^2}{dT} = -\frac{2\kappa(T)\Lambda_{net}(T, \Xi)}{\sigma_T^2}. \quad (7)$$

A steady-state requires vanishing heat flux at both boundaries of the transition layer, or

$$y^2|_{T=T_1} - y^2|_{T=T_2} = 0 = -2 \int_{T_1}^{T_2} \frac{\kappa(T)\Lambda_{net}(T, \Xi)}{\sigma_T^2} dT, \quad (8)$$

where T_1 and T_2 are the temperatures of the two stable phases which are connected by a transition layer. This condition determines a unique ionization parameter Ξ for the transition layer in question, and the integration of Equation (7) along the vertical height gives the detailed temperature profile as a function of optical depth.

If the disk does not realize the steady-state solution, there are additional enthalpy terms in Equation (2) which require that there be mass flow through the transition region – i.e. the cool material in the disk evaporates, or the hot material in the corona condenses (Meyer & Meyer-Hofmeister 1994; Dullemond 1999; Różańska & Czerny 2000b). Physically, this corresponds to a movement of the transition layer up or down through the vertical disk structure. However, since the density increases monotonically toward the center of the disk, this “motion” stops where the transition layer reaches the steady state value of Ξ . Thus, in the absence of disk winds or continuous condensation from a disk corona, the steady state solution should generally be obtained.

2.2.2. The Intermediate Stable Layer

There is a complication for the “S-curves” shown in Figure 1, because in each curve there exist two unstable regions and therefore there should be two transition layers. For “S curve 1”, Condition 8 can be met for both transition layers with resulting ionization parameters $\Xi_1 < \Xi_2$, where Ξ_1 and Ξ_2 are associated with the transition layer which connects to the lowest temperature phase and highest temperature phase, respectively. For “S curve 2”, the resulting ionization parameters for two transition layers, however, satisfy $\Xi_1 > \Xi_2$. Such a situation is unphysical, where the ionization parameter of the upper transition layer is smaller than that of the lower one, because in the context of accretion disks, the upper layer receives more ionizing flux and has lower pressure. So in practice, for “S curve 2” the intermediate stable region is skipped and a transition layer connects the lowest temperature phase to the highest temperature phase directly. The ionization parameter of this transition layer is determined the same way by applying Equation (8).

There is then an intermediate stable layer, of nearly uniform temperature, in between these two transition layers for “S curve 1”, as indicated with BC in Figure 1. The thickness of the intermediate layer should in principle be obtained by solving the coupled equations of hydrostatic equilibrium, energy balance, and radiative transfer. However, unlike the stable phase at the disk base or that of the corona, which may be Compton thick, this intermediate stable layer is generally optically thin, because its optical depth is restricted by the difference between Ξ_1 and Ξ_2 . Furthermore, the temperature in this layer is slowly varying, and therefore heat conduction can be neglected. We shall make another approximation that the variation of the force density F in the hydrostatic equation can also be neglected. This may not be a good approximation. However, since our main purpose is to investigate qualitatively the effects of an intermediate stable layer, such a simplifying procedure does capture the proper scaling relations of the problem, and has the advantage of less specific

model dependence. Writing Equation (1) in a dimensionless form and parameterizing the force factor by a dimensionless parameter $A = cF/\sigma_T F_x$, we obtain

$$\frac{1}{\Xi^2} \frac{d\Xi}{d\tau_e} = A. \quad (9)$$

The parameter A defined here is identical to the gravity parameter in Nayakshin, Kazanas & Kallman (2000) in the absence of radiation pressure. The integration of this equation from Ξ_1 to Ξ_2 gives the Thomson depth of the intermediate stable layer.

Assuming radiation pressure can be neglected, The force factor at a given radius R of the disk can be estimated as

$$A = \frac{1}{l} \frac{H}{R} \frac{4\pi GMm_p c}{\sigma_T L_{EDD}}, \quad (10)$$

where l is the luminosity of the continuum source in units of the Eddington limit, H is the half thickness of the disk at radius R , M is the mass of the central source, m_p is the proton mass, and L_{EDD} is the Eddington luminosity. In this estimate, we have assumed that $F_x = L/4\pi R^2$. This gives A the value:

$$A = 1.4 \frac{1}{l} \frac{H}{R}. \quad (11)$$

For a typical thin disk, as those present in AGN and black hole binaries, one expects $H/R \sim 0.01$. If the luminosity is sub Eddington, $l \sim 0.01$ as in most AGNs, A is of order unity. However, since the disk surface may not be normal to the continuum radiation, F_x may be only a fraction of the value assumed above, which increases A by one or two orders of magnitude. On the other hand, as the source approaches the Eddington limit, A may become smaller than 1. Therefore, we expect A to be in the range of 0.1 – 10. The exceptional cases of much smaller and larger A are discussed in §4.

The temperature profiles and optical depths of the transition layers and possible intermediate stable layer are shown in Figures 2. Three labeled curves in solid lines correspond to “S-curve 1” (in Figure 1) with different values of the force factors $A = 10$,

1, and 0.1, respectively. The dashed curve corresponds to “S-curve 2”, where there is no intermediate stable layer. For each of the solid curves, three layers are clearly seen, with two transition layers being connected by an intermediate stable layer, as illustrated for the case of $A = 1$. The smaller A produces a more extended intermediate stable layer as expected.

EDITOR: PLACE FIGURE 2 HERE.

3. X-RAY EMISSION AND RESONANCE LINE SCATTERING

3.1. X-ray Emission From Radiative Recombination (RR)

Because the stable phase with the lowest temperature is almost neutral, and the stable phase at the highest temperature is almost fully ionized, they are not efficient in generating X-ray line emission, except for iron fluorescence lines from the neutral material. Only the transition layers and the intermediate stable layer are expected to emit discrete lines in the soft X-ray band. In a photoionized plasma, the temperature is too low for collisional excitation to be an important line formation process. Instead, radiative recombination (RR) followed by cascades dominates the line emission. The flux of a particular line can be written as

$$F_{em} = \int n_e n_i E_l \Lambda_l(T) dx, \quad (12)$$

where n_i is the density of the ion before recombination, E_l is the line energy, and $\Lambda_l(T)$ is the line emissivity defined as in Sako et al. (1999).

In ionization equilibrium where the ionization rate is equal to the recombination rate, we have $n_e n_i \alpha_i = n_{i-1} \int \frac{F_x(E)}{E} \sigma_{i-1}(E) dE$, where α_i is the recombination coefficient of ion i , n_{i-1} is the number density of ion $i - 1$, $F_x(E)$ is again the monochromatic incident flux (differential in energy), and $\sigma_{i-1}(E)$ is the photoionization cross section of ion $i - 1$.

Defining the branching ratio $\rho_l(T) = \frac{\Lambda_l}{\alpha_i}$, Equation (12) can be rewritten as:

$$F_{em} = E_l \int \frac{F_x(E)}{E} \frac{\sigma_{i-1}(E)}{\sigma_T} dE \int \rho_l(T) f_{i-1}(\Xi, T) d\tau_e, \quad (13)$$

where $f_{i-1}(T, \Xi) = \frac{n_{i-1}}{n_e}$ is the fractional abundance of ion $i - 1$ with respect to the electron density.

As indicated, ρ_l and f_{i-1} depend only on temperature T and ionization parameter Ξ , which are both functions of optical depth τ_e . For convenience, we further define the “emission equivalent width” $EW_l^e = \frac{F_{em}}{F_x(E_l)}$. Then if $h(E) = \frac{F_x(E)}{F_x(E_l)}$, which depends only on the shape of the incident continuum, EW_l^e can be written as:

$$EW_l^e = E_l \int \frac{h(E)}{E} \frac{\sigma_{i-1}(E)}{\sigma_T} dE \int \rho_l(T) f_{i-1}(T, \Xi) d\tau_e. \quad (14)$$

Therefore the emission equivalent width EW_l^e is independent of the density of the medium and the incident flux. It is a unique function of the structure deduced in Section 2. All other variables depend only on T and Ξ . The numerical values of $\rho_l(T)$ were provided by D. Liedahl (private communication), and were calculated using the models described in Sako et al. (1999). The values of $f_{i-1}(T, \Xi)$ were computed using XSTAR (Kallman & Krolik 1986).

In Figure 3, we plot the spectra of the recombination emission within the 0.5 – 1.5 keV band with a spectral resolution ~ 2 eV, which is close to the spectral resolution of the grating spectrometers on *Chandra* and *XMM-Newton*. The top panel corresponds to the case without an intermediate stable layer, and the bottom panels corresponds to the case with an intermediate layer for $A = 10, 1$ and 0.1 , respectively. For clarity, from top to bottom, the flux in each panel is multiplied by a factor indicated in each panel. It appears that the existence of an intermediate stable layer enhances the emission in this energy band. This is not surprising since the ions that are responsible for these lines have peak abundances at temperatures close to that of the intermediate stable layer. In all cases,

the equivalent widths (EWs) of the emission lines are less than 1.0 eV, with respect to the ionizing continuum. The strongest lines are the hydrogen-like and helium-like lines of oxygen, with EWs approaching several tenths of an eV. Hydrogen-like and helium-like lines from iron outside the plotted energy band are somewhat stronger, with EWs reaching a few eV. We note that our low equivalent width values conflicts with those derived by Nayakshin, Kazanas & Kallman (2000), who found some lines with equivalent widths as high as 30 eV. However, since they did not consider the appropriate locations for the transition regions in Ξ -space, their intermediate stable layer subtended a much larger optical depth than we find here. Naturally with a thicker layer, they found larger equivalent widths.

EDITOR: PLACE FIGURE 3 HERE.

3.2. X-ray Reflection From Resonance Scattering (RS)

Emission from RR is not the only line formation process in the transition layers and the intermediate stable layer. Due to very large cross sections in resonance line scattering, the reflected flux in these lines may be significant. With the computed thermal and ionization structure, the column density in each ion and the optical depth in all resonance lines can be calculated straightforwardly.

The cross sections for resonance line scattering depend on the line broadening. We assume thermal Doppler effects as the only mechanism. Although the gas temperature is a function of depth, we calculate the line width for a temperature where the abundance of each ion peaks as an average, and assume that the resonance scattering cross sections are uniform along the vertical direction. In terms of absorption oscillator strength f , this cross

section of the resonance line scattering σ_{RS} can be written as

$$\sigma_{RS} = \frac{\pi e^2}{m_e c^2} f \frac{\lambda^2}{\Delta\lambda}, \quad (15)$$

where m_e is the electron mass, e is the electron charge, λ is the wavelength of the line and $\Delta\lambda$ is the average line width in wavelength. Under the assumption of thermal Doppler broadening,

$$\Delta\lambda = 2.35\lambda \sqrt{\frac{kT_M}{m_i c^2}}, \quad (16)$$

where T_M is the temperature at which the ion abundance peaks, and m_i is the ion mass.

The resonance scattering optical depth τ_{RS} for a line from ion i can be estimated as

$$\tau_{RS} = \sigma_{RS} N_i, \quad (17)$$

where N_i is the column density of the ion.

The radiative transfer in the line is a complicated issue (Dumont, Abrassart & Collin 2000). A full treatment is beyond the scope of this work. However, since we are only interested in a reasonable estimate of the reflected line flux, a simple approach may be adopted. We assume the resonance line scattering is isotropic and conservative and neglect the polarization dependence. Under such conditions, the reflection and transmission contributions by a plane-parallel slab of finite optical depth τ have been solved by Chandrasekhar (1960). For normal incident flux F_x , the angle dependent reflectivity is

$$r(\mu) = \frac{I}{F_x} = \frac{S(\tau, \mu)}{4\pi\mu}, \quad (18)$$

where $\mu = \cos\theta$, $r(\mu)$ is the reflectivity at μ , I is the reflected intensity, F_x is the incident flux, and $S(\tau, \mu)$ is the scattering function defined as

$$(1 + \frac{1}{\mu})S(\tau, \mu) = X(\mu)X(1) - Y(\mu)Y(1), \quad (19)$$

where $X(\mu)$ and $Y(\mu)$ are two functions that satisfy the following integral equations:

$$\begin{aligned} X(\mu) &= 1 + \frac{\mu}{2} \int_0^1 \frac{1}{\mu + \mu'} [X(\mu)X(\mu') - Y(\mu)Y(\mu')] d\mu' \\ Y(\mu) &= e^{-\tau/\mu} + \frac{\mu}{2} \int_0^1 \frac{1}{\mu - \mu'} [Y(\mu)X(\mu') - X(\mu)Y(\mu')] d\mu'. \end{aligned} \quad (20)$$

The solutions of these equations may be obtained by an iterative method with the starting point $X(\mu) = 1$ and $Y(\mu) = e^{-\tau/\mu}$. The angle integrated reflectivity R_t can be calculated as

$$R_t = 2\pi \int_0^1 r(\mu) \mu d\mu, \quad (21)$$

and is shown in Figure 4 as a function of the resonance scattering optical depth τ_{RS} .

EDITOR: PLACE FIGURE 4 HERE.

The reflected flux in a line can be written as

$$F_r = R_t F_x(E) \Delta E, \quad (22)$$

where ΔE is the line width in energy. Similarly to the “emission equivalent width” EW_l^e , we define a “reflection equivalent width” $EW_l^r = \frac{F_r}{F_x(E_l)}$, which results in:

$$EW_l^r = \frac{R_t \Delta \lambda h c}{\lambda^2}. \quad (23)$$

This “reflection equivalent width” from our numerical results is a few tenths of an eV for strong resonance lines, similar to that of the recombination emission lines.

In Figure 5, we plot the spectra of the resonantly scattered lines in the energy band 0.5 – 1.5 keV with a spectral resolution ~ 2 eV. The top panel corresponds to the case without an intermediate stable layer, and the bottom panels corresponds to the case with an intermediate layer for $A = 10, 1$ and 0.1 , respectively. For clarity, from top to bottom, the flux in each panel is multiplied by a factor of 100. We see that the equivalent widths of

the reflected lines are notably enhanced when there is an intermediate stable layer, but not as significantly as for the recombination emission lines. This is because the optical depths of many strong lines become much larger than unity, and the reflection is saturated. If there are broadening mechanisms other than thermal Doppler effects, such as turbulent velocity, the reflected intensity can be further enhanced.

EDITOR: PLACE FIGURE 5 HERE.

3.3. X-ray Spectrum with RR Emission and RS Reflection

In order to gain a crude idea of the relative importance of recombination emission and reflection from the transition layers and intermediate stable layer, we compare them to the “hump” produced by Compton scattering off a cold surface (Lightman & White 1988). We use the Greens function obtained by Lightman & White (1988) to calculate the Compton reflection. This method was verified to be accurate with a Monte Carlo procedure by George & Fabian (1991). In Figure 6, we show the combined spectra including recombination emission and reflection lines from resonance line scattering, and the Compton reflection “hump”.

EDITOR: PLACE FIGURE 6 HERE.

4. SUMMARY

We now summarize the most important conclusions that can be drawn from the calculations presented in this paper. We also discuss the detectability of the predicted line features.

1. The unique ionization parameters that characterize the steady-state solutions of the transition layers depend on the shape of the “S-curve”. We have shown that two power-law illuminating spectra with different high energy cutoffs produce very different temperature profiles. The harder spectrum only allows one transition layer even though there are two unstable branches in the “S-curve”, while the softer one allows two separate transition layers connected by an intermediate stable layer. This is due to the fact that the ionization parameter of the upper transition layer must be larger than that of the lower one, if they are to exist separately in a disk environment. The harder spectrum produces a turnover point of the upper branch of the “S-curve” at smaller Ξ . Therefore the transition layer due to the upper unstable region joins the lower one smoothly without allowing the intermediate stable region to form. The turnover of the upper “S-curve” represents the point where Compton heating starts to overwhelm bremsstrahlung. The ionization parameter at which this point occurs is related to the Compton temperature of the continuum, $\Xi_{top} \propto T_{IC}^{-3/2}$ (Krolik, McKee & Tarter 1981; Nayakshin 2000). A harder spectrum has larger T_{IC} , therefore the intermediate stable layer tends to disappear for hard incident spectra.
2. Although the Thomson depths of the transition layers and possible intermediate stable layer are generally negligible, the X-ray emission lines from them may comprise the main observable line features, because the temperatures of these layers are inaccessible to the stable phases, and thus some of the important lines can have appreciable emissivity only in these layers. Due to the much larger cross sections for resonance line scattering, reflection due to resonance lines off such transition layers is also important. The strengths of reflected lines are at least comparable with those of the recombination emission lines when there is no intermediate stable layer. Because the appearance of the reflected line spectrum is different from that of the recombination emission spectrum, high resolution spectroscopic observations should

be able to distinguish these mechanisms.

3. The justification of the assumption that the ionizing continuum does not scatter in the intermediate layer depends on the magnitude of the parameter A . The Thomson depth of this layer τ_e is given by:

$$\tau_e = \frac{1}{A} \left(\frac{1}{\Xi_1} - \frac{1}{\Xi_2} \right). \quad (24)$$

For the power-law continuum with high energy cutoff at 150 keV (“S curve 1”), $\Xi_1 = 2.82$ and $\Xi_2 = 3.14$ from our numerical results. Therefore, $\tau_e = 0.036/A$. τ_e is much less than unity as long as A is greater than 0.1. For smaller A , however, another effect comes into play. Nayakshin, Kazanas & Kallman (2000) showed that the Thomson depth of the coronal layer (the stable phase with highest temperature) exceeds unity when the gravity parameter (identical to A defined here when the radiation pressure is neglected) is ~ 0.01 . Therefore not much ionizing flux can penetrate this layer, and the reprocessing in the deeper and cooler layers can be neglected completely. As A becomes much larger than 10, the thickness of the intermediate stable layer is negligible compared to the transition layers. Therefore, its presence may be ignored.

4. Since the recombination rate must equal the photoionization rate in the irradiated gas, recombination radiation is also a form of reflection – i.e. the line equivalent widths are independent of the incident flux. They depend only on the structure $(T(\tau); \Xi(\tau))$ deduced from the hydrostatic and energy balance equations.
5. The detectability of these recombination emission and reflection lines depends on whether the primary continuum is viewed directly. When the ionizing continuum is in direct view, our results show that the EWs of the strongest lines in the 0.5 – 1.5 keV band are at most a few tenths of an eV, slightly larger when there is an intermediate stable layer.

The signal to noise ratio (SNR) in such a line can be written as

$$SNR = \frac{EW}{E_l} (tE_l F_\gamma)^{1/2} \left(A_{eff} \frac{E}{\delta E} \right)^{1/2}, \quad (25)$$

where t is the integration time of the observation, E_l is the energy of the line, F_γ is the photon flux in the continuum, A_{eff} and $E/\delta E$ are the effective area and resolving power of the instrument, respectively. For a line at ~ 1 keV, with $EW = 1eV$, and with HETGS on board *Chandra*, we have $SNR = 0.25\sqrt{tF_\gamma}$. A typical Seyfert 1 galaxy has a flux of 10^{-10} erg cm $^{-2}$ s $^{-1}$ in the energy band of 2–10 keV. Assuming a power law with energy index of 1, the photon flux at 1 keV would be ~ 0.05 cm $^{-2}$ s $^{-1}$ keV $^{-1}$. For a reasonable integration time of 10 ks, we have $SNR \sim 5$. When the primary continuum is obscured as in Seyfert 2 galaxies, the EWs of the emission and reflection lines can be orders of magnitude larger, because the continuum at this energy region is absorbed severely, and the SNR can be greatly enhanced, making these lines observable.

Acknowledgment: SMK acknowledges several grants from NASA which partially supported this work, MFG acknowledges the support of a Chandra Fellowship at MIT. We wish to thank M. Sako, D. Savin and E. Behar for several useful discussions.

References

Chandrasekhar, S. 1960, Radiative Transfer, New York: Dover

Dullemond, C. P. 1999 *A&A* 341, 936

Dumont, A. M., Abrassart, A., & Collin, S. 2000 *A&A* 357, 823

Field, G. B. 1965, *ApJ* 142, 531

George, I. M., & Fabian, A. C. 1991, *MNRAS* 249, 475

Kallman, T. R., & Krolik, J. H. 1986, NASA/GSFC Laboratory for Heigh Energy Physics spec. rep.

Krolik, J. H., McKee, C. F., & Tarter, C. B. 1981, *ApJ* 249, 422

Lightman, A. P., & White, T. R. 1988, *ApJ* 335, 57

Matt, G., Fabian, A. C., & Ross, R. R. 1993, *MNRAS* 262, 179

Meyer, F., & Meyer-Hofmeister, E. 1994, *A&A* 288, 175

Nayakshin, S. 2000, *ApJ* 534, 718

Nayakshin, S., Kazanas, D., & Kallman, T. R. 2000, *ApJ* 537, 833

Ross, R. R., & Fabian, A. C. 1993, *MNRAS* 261, 74

Ross, R. R., Fabian, A. C., & Brandt, W. N. 1996, *MNRAS* 278, 1082

Ross, R. R., Fabian, A. C., & Young, A. J. 1999, *MNRAS* 306, 461

Róžańska, A. 1999, *MNRAS* 308, 751

Róžańska, A., & Czerny, B. 2000a, *MNRAS* 316, 473

Różańska, A., & Czerny, B. 2000b, *A & A* 360, 1170

Sako, M., Liedahl, D. A., Kahn, S. M., & Paerels, F. 1999, *ApJ* 525, 921

Shakura, N. I., & Sunyaev, R. A. 1973, *A & A* 24, 337

Spitzer, L. 1962, *Physics of Fully Ionized Gases*, New York: Interscience

Zel'dovich, Y. B., & Pikel'ner, S. B. 1969, *JETP* 29, 170

Życki, P. T., Krolik, J. H., Zdziarski, A. A., & Kallman, T. R. 1994, *ApJ* 437, 597

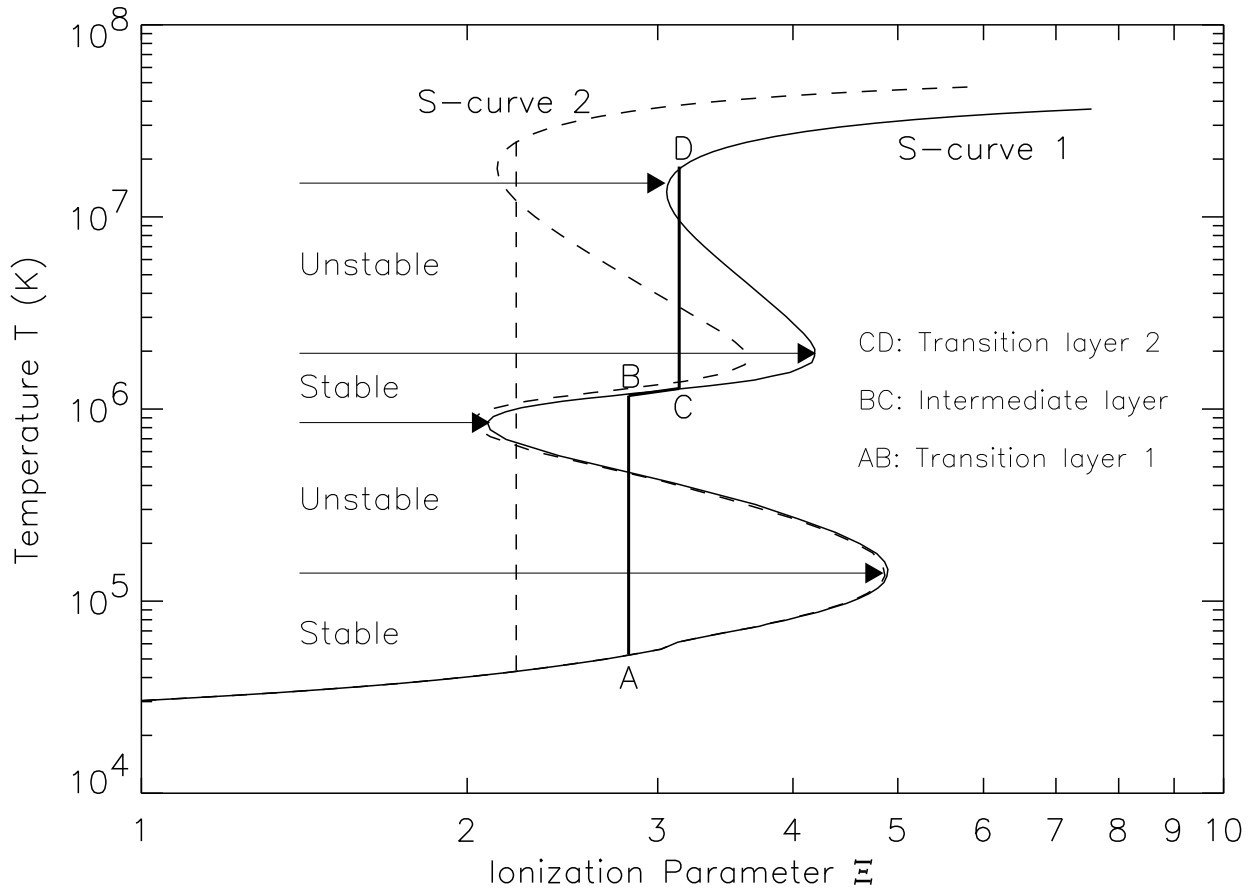


Fig. 1.— The “S-curves” produced by two different incident ionizing spectra. The vertical line indicates the unique solution of Ξ which satisfies Condition 8: two solutions for “S-curve 1”, $\Xi_1 = 2.82$ and $\Xi_2 = 3.14$; and only one for “S-curve 2”, $\Xi = 2.22$.

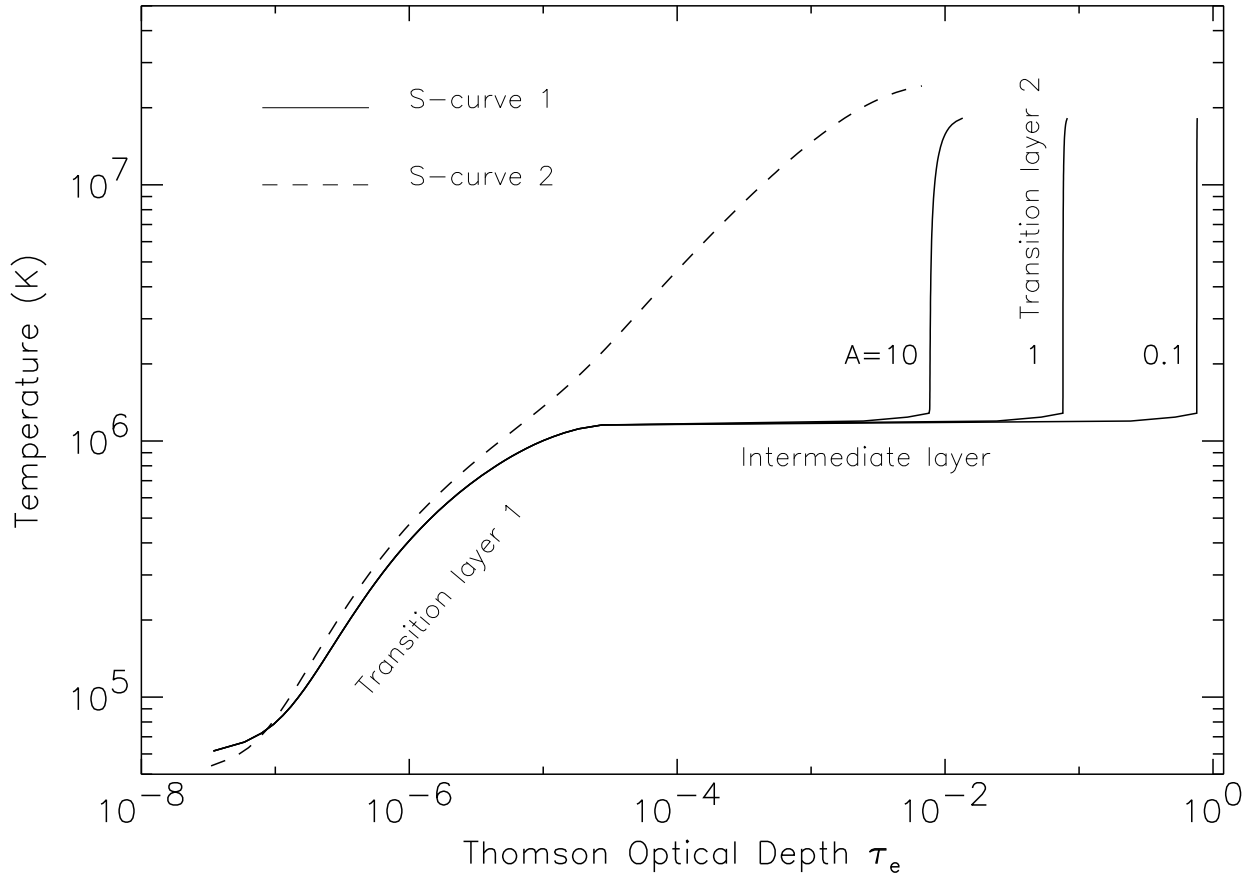


Fig. 2.— The temperature profiles of the transition layers and the intermediate stable layer versus Thomson optical depth τ_e . The solid curves correspond to “S-curve 1” with different force factors A , the dashed line corresponds to the “S-curve 2”.

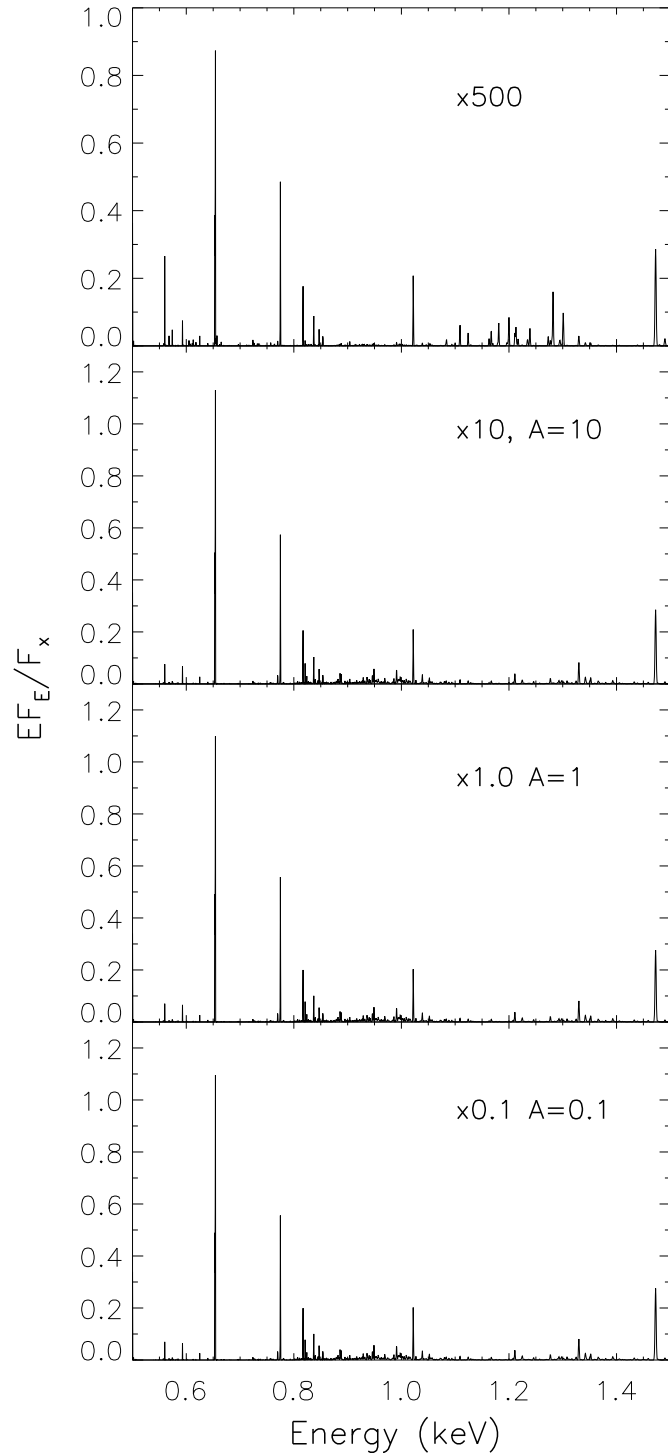


Fig. 3.— The spectra of the emission lines via RR in the transition layers and the intermediate stable layer. The spectral resolution is $\Delta E \sim 2$ eV. The top panel corresponds to “S-curve 2”, while bottom panels correspond to “S-curve 1” with different parameter A.

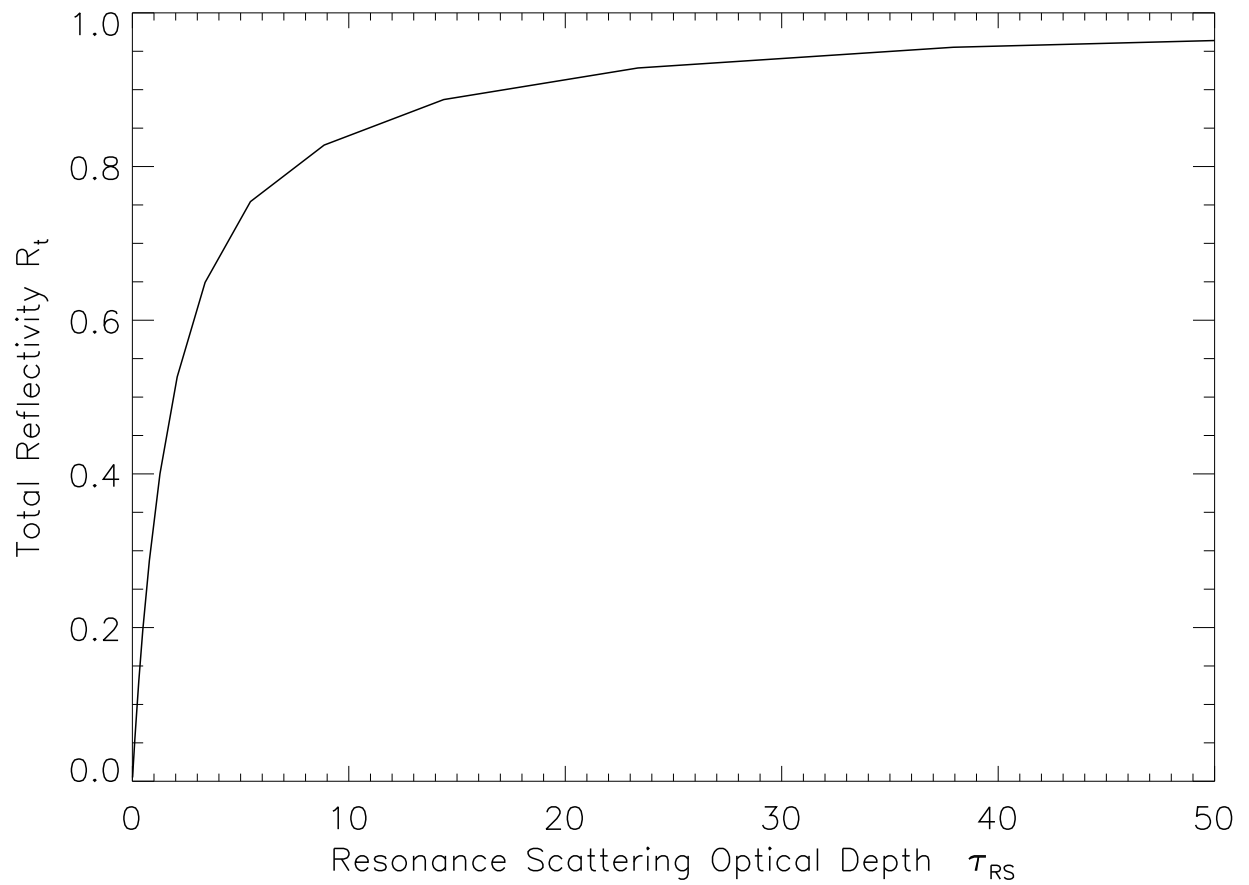


Fig. 4.— The angle integrated reflectivity of a plane parallel slab with normal incident flux as a function of the resonance scattering optical depth τ_{RS} .

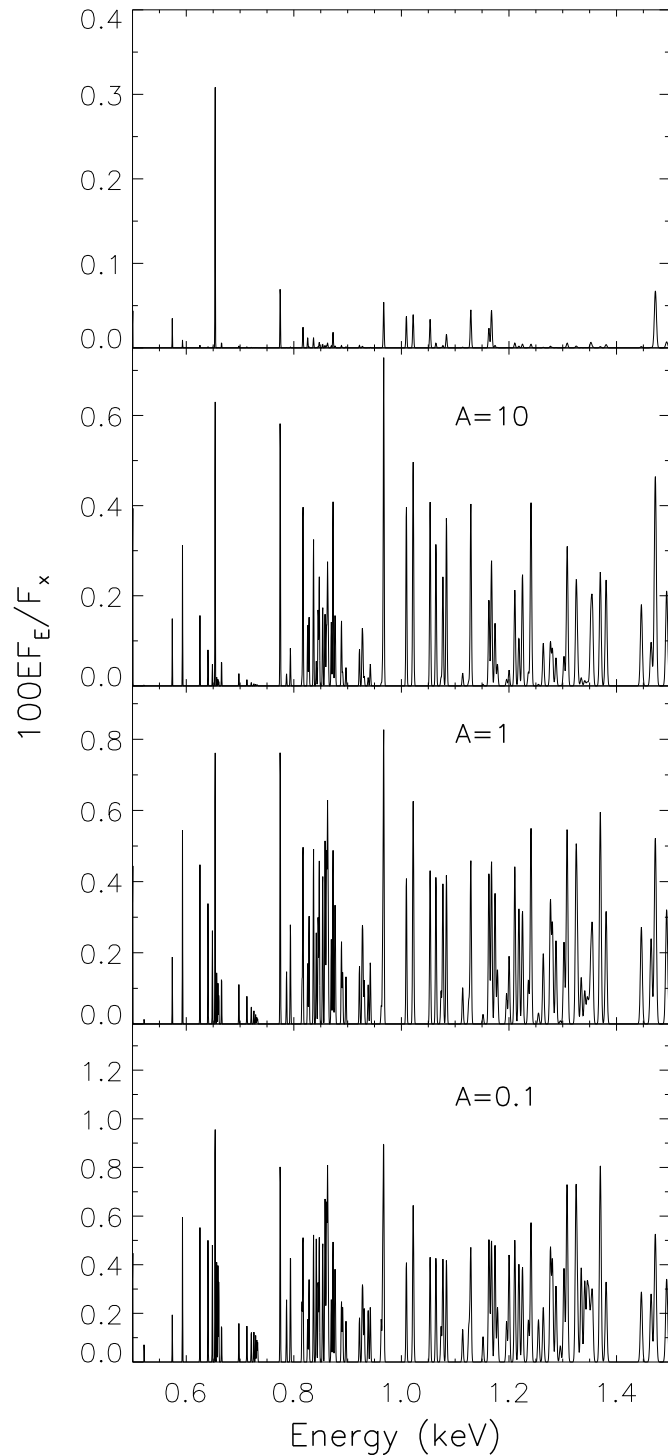


Fig. 5.— The spectra of the reflection lines due to resonance scattering in the transition layers and the intermediate stable layer. The spectral resolution is ~ 2 eV. The top panel corresponds to “S-curve 2”, while bottom panels correspond to “S-curve 1” with different parameter A.

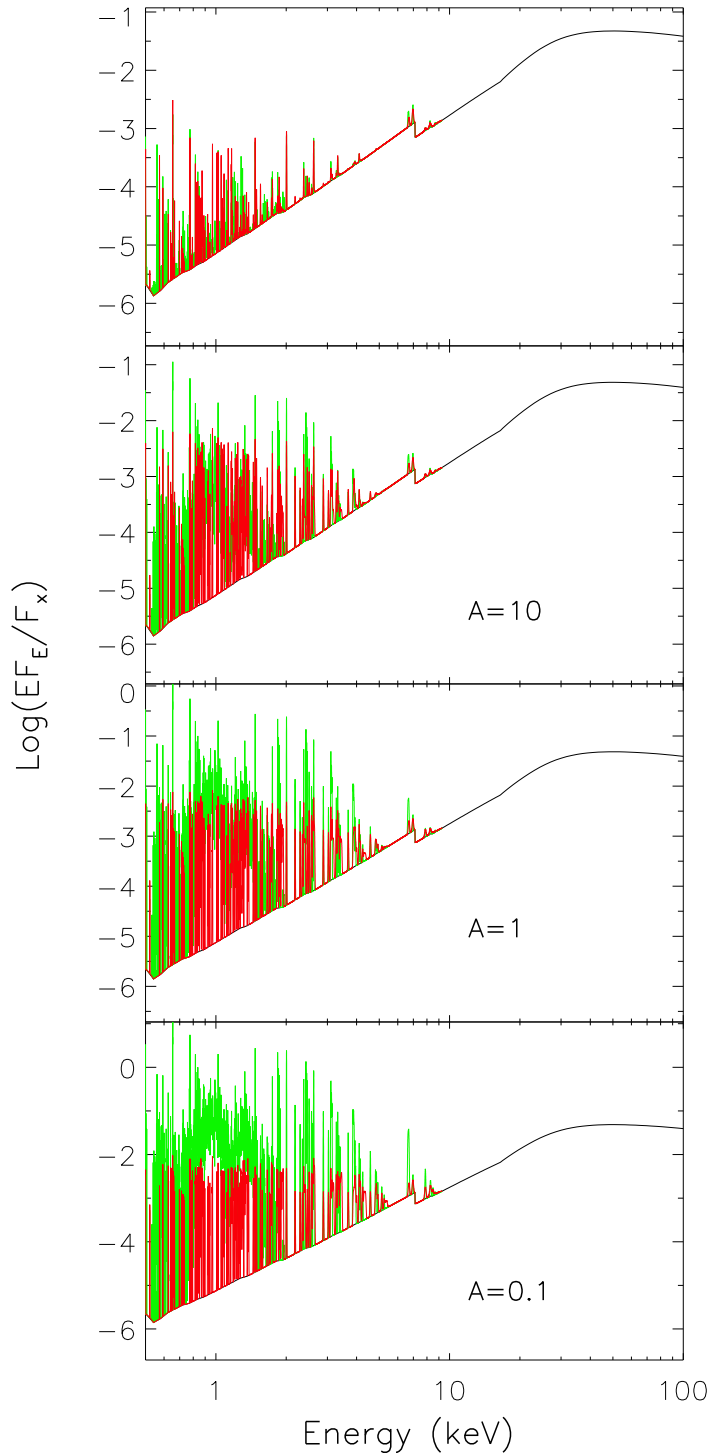


Fig. 6.— The combined spectrum. Green – emission lines via recombination, red – reflection lines due to resonance line scattering, and black – the Compton reflection hump. The spectral resolution is ~ 2 eV. The top panel corresponds to “S-curve 2”, while bottom panels correspond to “S-curve 1” with different parameter A.